C. R. Mecanique 343 (2015) 571–579

Contents lists available at ScienceDirect

Comptes Rendus Mecanique

www.sciencedirect.com

Discrete simulation of fluid dynamics

Study of hydrodynamic instabilities with a multiphase lattice Boltzmann model

Ali Mauricio Velasco *, José Daniel Muñoz

Universidad Nacional de Colombia, Physics Department, Colombia

ARTICLE INFO

Article history:
Received 8 December 2014
Accepted 29 July 2015
Available online 14 August 2015

Keywords:
Lattice Boltzmann
Multiphase flow
Hydrodynamic instabilities
Atwood number

ABSTRACT

Rayleigh–Taylor and Kelvin–Helmholtz hydrodynamic instabilities are frequent in many natural and industrial processes, but their numerical simulation is not an easy challenge. This work simulates both instabilities by using a lattice Boltzmann model on multiphase fluids at a liquid-vapour interface, instead of multicomponent systems like the oil–water one. The model, proposed by He, Chen and Zhang (1999) [1] was modified to increase the precision by computing the pressure gradients with a higher order, as proposed by McCracken and Abraham (2005) [2]. The resulting model correctly simulates both instabilities by using almost the same parameter set. It also reproduces the relation $\gamma \propto \sqrt{A}$ between the growing rate γ of the Rayleigh–Taylor instability and the relative density difference between the fluids (known as the Atwood number A), but including also deviations observed in experiments at low density differences. The results show that the implemented model is a useful tool for the study of hydrodynamic instabilities, drawing a sharp interface and exhibiting numerical stability for moderately high Reynolds numbers.

1. Introduction

Hydrodynamic instabilities are very common processes in daily life. The clouds of periodic curls in a sunny day, how the water jet from the tap breaks into droplets and the beautiful mushroom-like patterns that can be seen when the coffee mixes with water are some examples of hydrodynamic instabilities. Hydrodynamic instabilities use to appear when two fluids in contact generate a metastable interface. Due to the involved forces, an initial perturbation grows to form complex structures with certain grade of periodicity. As a matter of fact, perturbations with a specific wavelength grow faster than others and, in consequence, their evolution will generate periodic patterns with that wavelength. This is the secret behind the shape of the jet contrails that break into similar puffs, the periodicity of droplets at the ceiling of the shower or the geometric structure of supernovas. In addition, hydrodynamic instabilities are relevant in many industrial processes, not only as undesirable phenomena, as in the field of inertial confinement fusion where instabilities reduce the fusion rate, but also as something that can be useful to create homogeneous drops and grains. Even more, the set of differential equations governing the behaviour of hydrodynamic instabilities are common to other fields of non-linear dynamics (as plasma physics and general relativity); therefore, they use to be handled as paradigms to investigate other non-linear—but hardly reproducible—systems. The equations used to describe the hydrodynamic instabilities are non-linear partial differential equations, and their analytical solution is only plausible for the simpler cases. For all others it is necessary to use computational methods.

* Corresponding author.
E-mail addresses: amvelascos@unal.edu.co (A.M. Velasco), jdmunozc@unal.edu.co (J.D. Muñoz).

http://dx.doi.org/10.1016/j.crme.2015.07.014
1631-0721/

Multiphase lattice-Boltzmann models (MLBM), unlike other numerical methods, do not discretize the differential equations of fluid mechanics, but they simulate the transport and collision of the probability distributions for the molecules of the fluid. By adding interaction forces between the molecules, the fluid segregates into differentiated phases and the surface tension appears naturally. Thus, MLBM are specially appropriated to simulate hydrodynamic instabilities. The first MLBM was proposed in 1993 by Shan and Chen [3], who included interactions among particles. Through the adequate choice of interaction potentials, phase segregation occurs automatically. Next, He Shan and Doolen [4] obtained a more realistic equation of state by including two terms in the interaction potential: a strong short-range interaction, due to the volume exclusion among molecules, and a weak long-range component, from a Van der Waals mean-field approximation of the attractive forces. This proposal solves some thermodynamic inconsistencies of the Shan and Chen model and allows us to use the Maxwell's equal-area rule (see [5]). Later on, He, Chen and Zhang [1] included an index function (an extra set of distribution functions) to identify the two phases by a number, and used it to simulate the Rayleigh–Taylor instability (RTI). This index function improves the stability and keeps a sharp interface through the time evolution. More recently, Xu et al. [6] introduced a multiphase lattice-Boltzmann model with multiple relaxation times that simulates both the Kelvin–Helmholtz (KHI) and the Richmyer–Meshkov (RMI) instabilities, but it has a huge amount of parameters to be adjusted (actually, a different set for each instability), instead of including interparticle forcing terms, and the equation of state for the fluid has not being established yet.

Our aim is to simulate both the RTI and KHI via the lattice-Boltzmann model for a single-component multiphase system, i.e. a liquid-vapour configuration. For this purpose, we use the model introduced by He, Chen and Zhang, but using the hybrid scheme proposed by McCracken and Abraham [2] to calculate the pressure gradient, which improves accuracy and stability. In the next section, we describe the model. Section 3 contains our results for the RTI and KHI, where we focus on the effect of the parameters of the equation of state and the Atwood Number on the development of the instabilities and give a set of optimal parameters for the instability onset. Finally, our conclusions are summarized in Section 4, which also suggests future research works in this interesting area.

2. Model description

Standard lattice-Boltzmann models can be described by the continuous Boltzmann equation,

$$\frac{\partial f}{\partial t} + \boldsymbol{\xi} \cdot \nabla f = \frac{1}{\tau}(f^{(\mathrm{eq})} - f) \tag{1}$$

representing the propagation (left-hand side) and interaction or collision (right-hand side) of some distribution functions f, which can be taken as the probability of finding a particle with position $\boldsymbol{x}$ and velocity $\boldsymbol{\xi}$. Eq. (1) uses the BGK (Bhatnagar, Gross, Krook) approximation [7] in order to write the collision term in a simplified form. Here $f^{(\mathrm{eq})}$ is called the equilibrium distribution function (corresponding to a Maxwell–Boltzmann distribution) and τ is the relaxation time. By assuming a low-velocity regime and approximating the Maxwellian up to second order, the equilibrium distribution function takes the form

$$f^{(\mathrm{eq})} = \frac{\rho}{(2\pi RT)^{D/2}} \exp\left(-\frac{\boldsymbol{\xi}^2}{2RT}\right)\left[1 + \frac{(\boldsymbol{\xi}\cdot\boldsymbol{u})}{RT} + \frac{(\boldsymbol{\xi}\cdot\boldsymbol{u})^2}{2(RT)^2} - \frac{|\boldsymbol{u}|^2}{2RT}\right] \tag{2}$$

with D the dimension, R the ideal-gas constant and T the temperature. The quantities ρ and $\boldsymbol{u}$ are the density and macroscopic velocity at a given point, respectively. If time and space are discrete in steps δt and $\boldsymbol{x} + \boldsymbol{\xi}\delta_t$ respectively, Eq. (1) takes the form

$$f(\boldsymbol{x} + \boldsymbol{\xi}\delta_t, \boldsymbol{\xi}, t + \delta_t) - f(\boldsymbol{x}, \boldsymbol{\xi}, t) = -\frac{1}{\tau}\left[f(\boldsymbol{x}, \boldsymbol{\xi}, t) - f^{(\mathrm{eq})}(\boldsymbol{x}, \boldsymbol{\xi}, t)\right] \tag{3}$$

In this work, we set $\delta t = 1$, and the stability of the system is controlled by restricting the Reynolds number and the magnitude of the velocities in order to maintain the low-velocity assumption made above. Finally, the velocity space is chosen discrete in such a way that the macroscopic quantities

$$\rho = \sum_{i=1}^{n} f_i \qquad \rho\boldsymbol{u} = \sum_{i=1}^{n} f_i\xi_i \qquad 2\rho\varepsilon + \rho|\boldsymbol{u}|^2 = \sum_{i=1}^{n} f_i\xi_i^2 \tag{4}$$

where $\varepsilon = 3RT/2$ is the internal energy, which is maintained constant, with T the temperature and R the ideal gas constant, coincide with the density, the momentum and the energy computed from Gaussian quadrature up to second order in cell size, with one distribution function per discrete velocity, $f(\boldsymbol{x}, \boldsymbol{\xi_i}, t) = f_i$. An example of such a velocity set is D2Q9 (Fig. 1), which can be written as

$$\boldsymbol{\xi}_i = \begin{cases} \mathbf{0} & i = 0 \\ c\cdot\left(\cos\left[(i-1)\frac{\pi}{2}\right], \sin\left[(i-1)\frac{\pi}{2}\right]\right) & i = 1,2,3,4 \\ \sqrt{2}c\cdot\left(\cos\left[(i-5)\frac{\pi}{2} + \frac{\pi}{4}\right], \sin\left[(i-5)\frac{\pi}{2} + \frac{\pi}{4}\right]\right) & i = 5,6,7,8 \end{cases} \tag{5}$$

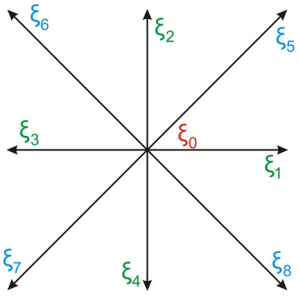

Fig. 1. (Colour online.) Set of discrete velocities d2q9.

where $c = \frac{\delta x}{\delta t} = \sqrt{3RT}$ is the magnitude of the evolution velocity to the four nearest lattice sites and will characterize, in this model, the lattice length (since $\delta t = 1$). The velocities weights

$$w_i = \begin{cases} 4/9 & i = 0 \\ 1/9 & i = 1, 2, 3, 4 \\ 1/36 & i = 5, 6, 7, 8 \end{cases} \tag{6}$$

are chosen to ensure isotropy in the model. The time evolution of this system should reproduce the behaviour of fluids in the macroscopic limit (that is, the Navier–Stokes equations of an ideal isothermal gas, with $p_{ideal} = \rho RT = \rho/3$ the pressure). However, in 2006, Philippi et al. [8] showed that this D2Q9 scheme is a second-order approximation of the continuous Boltzmann equation, while third-order approximations are necessary to recover the Navier–Stokes equations exactly. Nevertheless, this approximation is good enough for our work, since we are interested in the first stages of the evolution of the instabilities, without considering the turbulent regime where these high-order effects will be more appreciable.

In order to simulate multiphase systems, the above model should be modified to include inter-particle forces. In 1999, He, Chen and Zhang [1], based on the forcing term proposed by He Shan and Doolen [4] in 1998, developed a method that includes both capillary and gravitational forces, and it is able to simulate phase segregation with a very sharp interface by the inclusion of an index function. Let us start by considering an inter-particle force from a mean field van der Waals approximation with exclusion term

$$\boldsymbol{F} = \rho\nabla\left(2a\rho + \kappa\nabla^2\rho\right) - b\rho^2 RT\chi\nabla\ln\left(\rho^2\chi\right) \tag{7}$$

where a is an attractive parameter, κ is related to the surface tension, χ is the collision probability (which depends on the fluid density) $b = 2\pi\sigma^3/3m$ is the parameter corresponding to the short-range volume exclusion interaction and σ is the particle diameter [9]. The force can be written as

$$\boldsymbol{F} = -\nabla\left(b\rho^2 RT\chi - a\rho^2\right) + \kappa\rho\nabla\nabla^2\rho = -\nabla\psi + \boldsymbol{F}_s \tag{8}$$

where $\boldsymbol{F}_s$ is the surface tension; we have defined $\psi(\rho) := b\rho^2 RT\chi - a\rho^2$ the interparticular potential.

Due to the interparticle interaction included, the system is no longer an ideal gas; therefore, its thermal behaviour will be lead by a different equation of state that can be written as

$$p = \rho RT + b\rho^2 RT\chi - a\rho^2 \tag{9}$$

As a particular case of the above equation, in this work we use the Carnahan–Starling equation of state:

$$p = \rho RT\frac{1 + b\rho/4 + (b\rho/4)^2 - (b\rho/4)^3}{(1 - b\rho/4)^3} - a\rho^2 = \rho RT + \rho^2 RT\frac{4 - 2\rho}{(1-\rho)^3} - a\rho^2 \tag{10}$$

where we chose $b = 4$ for simplicity. Note that we can obtain Eq. (10) from Eq. (9) by making $\chi = \frac{4-2\rho}{4(1-\rho)^3}$ and $b = 4$. Now, from Eq. (9) and the definition of ψ, it is possible to write

$$p = \psi + \rho RT \tag{11}$$

or, equivalently

$$\psi = p - \rho RT \tag{12}$$

then, the potential ψ actually corresponds to the deviation of the pressure compared to the value it would take if the system were an ideal gas ($p_{\text{ideal}} = \rho RT$).

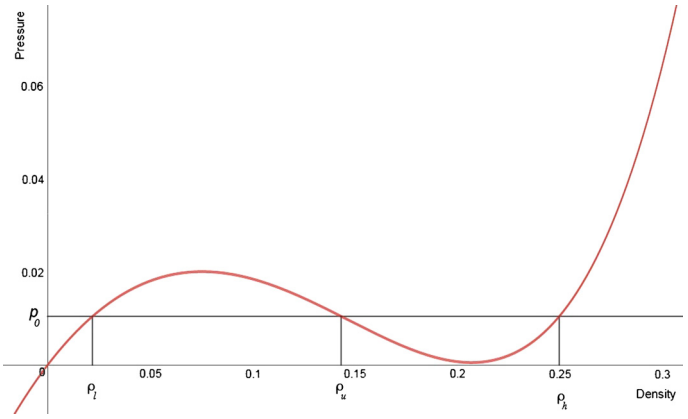

Fig. 2. (Colour online.) P–ρ diagram of the Carnahan–Starlin equation of state for a given temperature.

Eq. (10) allows the coexistence of three different densities at the same pressure p_0, as shown in Fig. 2 when $RT < 0.3773\,(a/b)$; two of them (ρ_l and ρ_h) will be mechanically stable and correspond to the densities of the two phases, the third one is mechanically unstable ρ_u and is responsible for phase segregation.

Including these forces (Eq. (8)) into the discrete lattice-Boltzmann equation (Eq. (3)) leads to

$$f_i\left(\boldsymbol{x}+\boldsymbol{\xi_i}\delta_t,\,\boldsymbol{\xi_i},\,t+\delta_t\right)-f_i\left(\boldsymbol{x},\,\boldsymbol{\xi_i},\,t\right)=\frac{1}{\tau}\left[f_i\left(\boldsymbol{x},\,\boldsymbol{\xi_i},\,t\right)-f_i^{(\mathrm{eq})}\left(\boldsymbol{x},\,\boldsymbol{\xi_i},\,t\right)\right]+\frac{(\boldsymbol{\xi}-\boldsymbol{u})\cdot(-\nabla\psi+\boldsymbol{F}_s+\boldsymbol{G})}{\rho RT}f_i^{(\mathrm{eq})}\left(\boldsymbol{x},\,\boldsymbol{\xi_i},\,t\right) \tag{13}$$

where $\boldsymbol{G}$ represents body forces like gravity.

Note that $-\nabla\psi$ is directly responsible for phase segregation, because the ideal gas pressure grows linearly with phase density and, therefore, the gradient of ψ is higher at the interface. As a consequence, the computations via finite differences induce large truncation errors at the interface, affecting the numerical stability. In order to reduce the impact of this truncation error, He et al. [1] introduced a new field

$$g_i=f_iRT+\psi\,(\rho)\,\Gamma_i\,(0) \tag{14}$$

which corresponds to a pressure distribution function, where

$$\Gamma_i\,(\boldsymbol{u})=w_i\left[1+\frac{3}{c^2}\boldsymbol{\xi}_i\cdot\boldsymbol{u}+\frac{9}{2c^4}\left(\boldsymbol{\xi_i}\cdot\boldsymbol{u}\right)^2-\frac{3|\boldsymbol{u}|^2}{2c^2}\right] \tag{15}$$

The evolution equation for this pressure distribution function is

$$\bar{g}_i\left(\boldsymbol{x}+\boldsymbol{\xi_i}\delta_t,\,\boldsymbol{\xi_i},\,t+\delta_t\right)-\bar{g}_i\left(\boldsymbol{x},\,\boldsymbol{\xi_i},\,t\right)=-\frac{1}{\tau}\left[\bar{g}_i\left(\boldsymbol{x},\,\boldsymbol{\xi_i},\,t\right)-g_i^{(\mathrm{eq})}\left(\boldsymbol{x},\,\boldsymbol{\xi_i},\,t\right)\right]+\frac{2\tau-1}{2\tau}\left(\boldsymbol{\xi}_i-\boldsymbol{u}\right)\cdot\left[\Gamma_i\,(\boldsymbol{u})\,(\boldsymbol{F}+\boldsymbol{G})-(\Gamma_i\,(\boldsymbol{u})-\Gamma_i\,(0)\,\nabla\psi\,(\rho)\right]\delta_t \tag{16}$$

The problematic gradient term in Eq. (16) is multiplied by $(\Gamma_i\,(\boldsymbol{u})-\Gamma_i\,(0)$, which, from Eq. (15), is on the order of the Mach number; thus, the calculation errors due to the high gradient at the interface are considerably reduced, since the Mach number is in general very small for both RTI and KHI. Eq. (16) includes the change of variable

$$\bar{g}_i\equiv g_i-\frac{1}{2}\left(\boldsymbol{\xi}_i-\boldsymbol{u}\right)\cdot\left[\Gamma_i\,(\boldsymbol{u})\,(\boldsymbol{F}_s+\boldsymbol{G})-(\Gamma_i\,(\boldsymbol{u})-\Gamma_i\,(0)\,\nabla\psi\,(\rho)\right]\delta_t \tag{17}$$

that keeps a discrete explicit scheme and simplify the calculations. The equilibrium distribution functions for this new field are

$$g^{(\mathrm{eq})}=w_i\left[p+\rho\left(1+\frac{3}{c^2}\boldsymbol{\xi}_i\cdot\boldsymbol{u}+\frac{9}{2c^4}\left(\boldsymbol{\xi_i}\cdot\boldsymbol{u}\right)^2-\frac{3|\boldsymbol{u}|^2}{2c^2}\right)\right] \tag{18}$$

with

$$p=\sum_i\bar{g}_i-\frac{1}{2}\boldsymbol{u}\cdot\nabla\psi\,(\rho)\,\delta_t\qquad\rho RT\boldsymbol{u}=\sum_i\xi_i\bar{g}_i+\frac{RT}{2}\,(\boldsymbol{F_s}+\boldsymbol{G})\,\delta_t \tag{19}$$

As we mentioned before, the non-ideal gas state equation allows the coexistence of different densities at the same pressure. For this reason, Eqs. (19) are not enough to completely determine the system, and it is necessary to include a new set of distribution functions $\bar{f}_i$ responsible for labelling the phases with a distinctive value

$$\phi = \sum_i \bar{f}_i \tag{20}$$

Therefore, there will be two initial values of ϕ, i.e. ϕ_l, to label the low-density gaseous phase and ϕ_h for the high-density liquid phase. These values have to be chosen to coexist at the same pressure, following the equation of state and the Maxwell equal areas rule (see Fig. 2). Furthermore, since the overall pressure is maintained constant during the whole simulation at value p_0, the values of ϕ remain close to the initial ones ϕ_l and ϕ_h for each phase far from the interface and at the mechanically unstable value ϕ_u at the interface, which is responsible for phase segregation.

Later on, via linear interpolation, we can find a unique density value for each phase. As far as the new distribution function tracks the behaviour of the phases, it should follow the same evolution equation as the pressure distribution function, even though the only force responsible for phase separation is the excess pressure gradient and, therefore, it will be the only force exerted over this new function, i.e.

$$\begin{aligned}\bar{f}_i\left(\boldsymbol{x}+\boldsymbol{\xi_i}\delta_t,\,\boldsymbol{\xi_i},\,t+\delta_t\right)-\bar{f}_i\left(\boldsymbol{x},\,\boldsymbol{\xi_i},\,t\right)=&-\frac{1}{\tau}\left[\bar{f}_i\left(\boldsymbol{x},\,\boldsymbol{\xi_i},\,t\right)-f_i^{(\mathrm{eq})}\left(\boldsymbol{x},\,\boldsymbol{\xi_i},\,t\right)\right]\\&-\frac{2\tau-1}{2\tau}\left(\boldsymbol{\xi}_i-\boldsymbol{u}\right)\cdot\nabla\psi\left(\phi\right)\Gamma_i\left(\boldsymbol{u}\right)\frac{\delta_t}{RT}\end{aligned} \tag{21}$$

with

$$\bar{f}_i = f_i + \frac{1}{2RT}\left(\boldsymbol{\xi}_i-\boldsymbol{u}\right)\cdot\nabla\psi\left(\phi\right)\Gamma_i\left(\boldsymbol{u}\right)\delta_t \tag{22}$$

The equilibrium distribution function is given by

$$f_i^{(\mathrm{eq})} = w_i\phi\left[1+\frac{3}{c^2}\boldsymbol{\xi}_i\cdot\boldsymbol{u}+\frac{9}{2c^4}\left(\boldsymbol{\xi_i}\cdot\boldsymbol{u}\right)^2-\frac{3|\boldsymbol{u}|^2}{2c^2}\right] \tag{23}$$

Since the distribution functions must be positive, from $f_0^{(\mathrm{eq})}$, we see that $|\boldsymbol{u}|$ has to be lower than $\sqrt{2/3}$, which restricts the maximum fluid velocity that can be simulated within this model. In some cases, it is possible to find values of $f_{i\neq 0}<0$, especially at high Reynolds numbers, which affect the stability of the numerical scheme. A solution to this problem is the imposition of an additional constraint to the evolution in order to follow the Boltzmann H theorem. This procedure is called entropic lattice-Boltzmann [10]. Nevertheless, this inclusion is not necessary here, since we are not interested in the turbulent regime of the instabilities.

The actual fluid density is related to ϕ by

$$\rho\left(\phi\right) = \rho_\mathrm{h} + \frac{\phi-\phi_\mathrm{l}}{\phi_\mathrm{h}-\phi_\mathrm{l}}\left(\rho_\mathrm{h}-\rho_\mathrm{l}\right) \tag{24}$$

Summarizing, the multiphase lattice-Boltzmann model with an index function tracking the interface consists of two coupled forced lattice-Boltzmann schemes (Eqs. (16) and (21)). They allow us to obtain the pressure and momentum through Eq. (19), and the density is computed from Eqs. (20) and (24). In addition, to increase stability and accuracy, we compute the excess pressure gradient as proposed by Mc. Cracken and Abraham [2], by computing a sixth-order central difference method combined with a fourth-order method based upon Taylor series expansions in velocity space

$$\begin{aligned}\partial_i\psi^{(1)} &= \frac{1}{60\,\delta_x}\left[-\psi_{(i-3,j)}+9\,\psi_{(i-2,j)}-45\,\psi_{(i-1,j)}+45'\,\psi_{(i+1,j)}-9\,\psi_{(i+2,j)}+\psi_{(i+3,j)}\right]+\mathcal{O}\left(\delta_x^6\right)\\ \partial_i\psi^{(2)} &= \frac{1}{36\,c\,\delta_x}\sum_{\alpha=1}^{9}\xi_{\alpha,i}\left[8\,\psi\left(\boldsymbol{x}+\boldsymbol{\xi}_\alpha\delta_t\right)-\psi\left(\boldsymbol{x}+2\,\boldsymbol{\xi}_\alpha\delta_t\right)\right]+\mathcal{O}\left(\delta_x^4\right)\end{aligned} \tag{25}$$

which get 75% and 25% weighting respectively $\partial_i\psi\left(\rho\right)=0.75\partial_i\psi^{(1)}+0.25\partial_i\psi^{(2)}$. This completes the model. With these modifications of the standard lattice-Boltzmann model, the Chapman–Enskog expansion leads to the macroscopic equations:

$$\frac{\partial\rho}{\partial t}+\nabla\cdot\left(\rho\boldsymbol{u}\right)=0 \tag{26}$$

$$\rho\left[\frac{\partial\boldsymbol{u}}{\partial t}+\left(\boldsymbol{u}\cdot\nabla\right)\boldsymbol{u}\right]=-\nabla p+\nabla\cdot\boldsymbol{\Pi}+G \tag{27}$$

where $\boldsymbol{\Pi}:=\rho\,\nu\left(\nabla\boldsymbol{u}+\left(\nabla\boldsymbol{u}\right)^{\mathrm{T}}\right)$ and $\nu:=\left(\tau-1/2\right)RT\delta t$ are respectively the stress tensor and the kinematic viscosity.

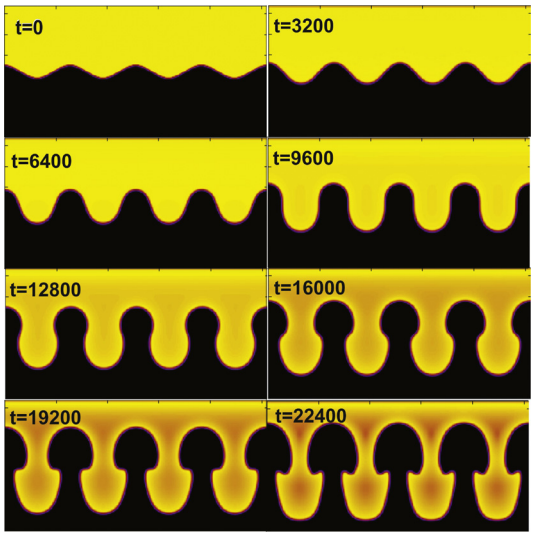

Fig. 3. (Colour online.) Evolution of the Rayleigh–Taylor instability. Time is given in computational time steps.

Even though this is not a thermal lattice-Boltzmann scheme, since temperature remains constant during the whole simulation, the quantity T plays a key role in phase segregation, since it requires to be chosen below a critical temperature to assure the existence of two different phases, as mentioned above, following the Carnahan–Starling equation of state (Eq. (10)).

As an important remark, note that even though we are not considering the high-order approximations in the advective term of the kinetic equation, the errors due to the possible thermodynamic inconsistencies of the model as studied by Wagner in 2006 [11] and Siebert et al. in 2014 [12] become more representative on systems with phase-segregation processes, but less influential when the system starts from two separated phases, as in our case. Even more, the inclusion of an index function actually generates a sharp interface, and our simulations show a uniform pressure at both sides of the interface, solving the two main drawbacks for thermodynamic inconsistency pointed out by Wagner; a thorough analysis of the correct retrieving of the coexistence curves, as pointed out by Siebert et al., is let for future work.

3. Results and discussion

The first step towards simulating the hydrodynamic instabilities is to find the stable values of the index function ϕ that allow the phases to co-exist. There are three possible values of ϕ: two of them, with $\frac{\partial p}{\partial \rho} > 0$, indicate the stable gas and liquid phases, ϕ_{l} and ϕ_{h}, respectively, while the third one, with $\frac{\partial p}{\partial \rho} < 0$, is mechanically unstable and generates phase segregation. The parameters of the model for the initial condition should be fitted in such a way that the index function for the two phases fulfills the Maxwell equal-area rule. A fine fit for the free parameters of the model lead us to set $a = 6.93$, $RT = a/12.00$, $\phi_{\mathrm{l}} = 0.0317$ and $\phi_{\mathrm{h}} = 0.2554$. Regarding surface tension, in the present work (and following the He, Chen and Zhang model to simulate the Rayleigh–Taylor Instability), we have chosen $\kappa = 0$, since the surface tension parameter uses to be very small in nature and, for the systems studied here, it can be neglected. In addition, although the surface tension is also present through interparticle interactions in a natural way, all our simulations show the same pressure at both sides of the interface. That is, the surface tension can be neglected in our simulations. Finally, we take the width of the computational domain W as the characteristic length scale of the system. The gravity was chosen to be the same as in the article by He Chen, and Zhang, $\sqrt{Wg} = 0.04$, and the time scale corresponds to $T = \sqrt{W/g}$. With this choice, the Reynolds number is $Re = \sqrt{Wg}W/\nu$. In the simulations, the Reynolds number was modified by maintaining W and g constant and varying the kinematic viscosity through the parameter τ.

Fig. 3 shows the evolution of an initially sinusoidal interface, with an amplitude h_0 and a wave number k. The heavier fluid has been placed above the lighter one, immersed in a gravitational field acting downwards. The initial condition for the index function reads

$$\phi(\boldsymbol{x}) = \frac{\phi_{\mathrm{h}} - \phi_{\mathrm{l}}}{\pi} \arctan\left(y - h_0 \cos(kx) - L_y/2\right) + \frac{\phi_{\mathrm{h}} + \phi_{\mathrm{l}}}{2} \tag{28}$$

where L_y is the height of the computational domain. The above initial distribution smooths the connection between the fluid densities, decreasing the numerical error that uses to appear at the interface.

At the first moments of the instability, the densest bubble grows without modifying its shape considerably. Then, the onset of vortices gives to the bubble a mushroom-like shape and slows its speed. Finally, the mushroom is enlarged, creating symmetrical jets on both sides (Fig. 3).

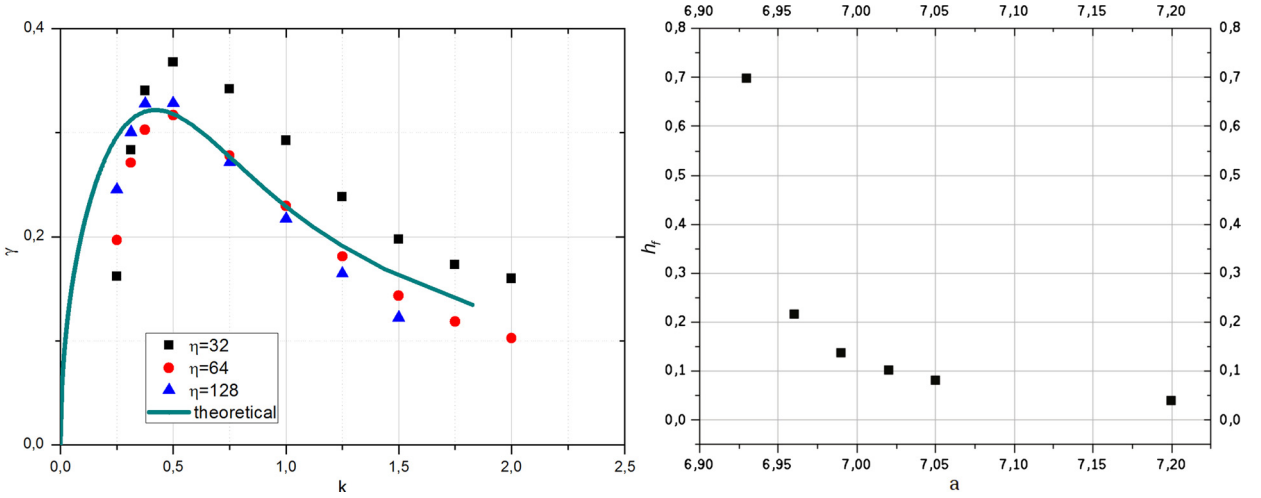

Fig. 4. (Colour online.) Growing rate γ as a function of the wavenumber for three different mesh heights η (left) and amplitude of the perturbation at a given time h_f as a function of the attractive parameter a (right).

We also studied the effect of the wave number k on the evolution of the instability. Fig. 4 (left) shows the relation between k and the growing rate γ for the Atwood Number, $A = \frac{\rho_h - \rho_l}{\rho_h + \rho_l} = 0.5$ where the sub-indexes "h" and "l" are related to the heavy and light fluids, respectively. Our results were compared with the theoretical relation proposed by Chandrasekhar in [13], which takes the form:

$$Q = \frac{y-1}{\alpha_h - \alpha_l}\left[y^3 + (1 + 4\alpha_l\alpha_h)\, y^2 + (3 - 8\alpha_l\alpha_h)\, y - (1 - 4\alpha_l\alpha_h)\right] \tag{29}$$

where $k = Q^{-1/3}$, $\gamma = \left(y^2 - 1\right) Q^{-2/3}$, $\alpha_l = \rho_l/(\rho_l + \rho_h)$, and $\alpha_h = \rho_h/(\rho_l + \rho_h)$. Even though the shape of the curves is almost the same, it can be observed a shift of the wavelength of the maximum instability that becomes lower when η is greater. This may be due to the fact that the implemented lattice-Boltzmann scheme is of the second order in cell size when third-order implementations are required to retrieve the Navier–Stokes equations. More proofs of the convergence of the method are required, but left for future studies. Note that a greater-size mesh gives a better location of the maximum, but the shape of the curve deviates from the theoretical one.

Once the method has been proved and a sharp interface has been achieved, we went further and studied the effect of the attractive parameter of the equation of state, since it is related to the internal composition of the fluids, expecting that a very high attractive parameter will prevent the fluids from mixing. Fig. 4 (right) shows how the value of the attractive parameter acts over the amplitude of the Rayleigh–Taylor instability for a given time, finding a strong dependence. The amplitude goes to zero if the attractive parameter is greater than 7.2, rapidly increasing if $a \approx 6.93$. In fact, if the attractive parameter is lower than 6.93, the mixture of the fluids occurs so quickly that our initial assumption of low velocities becomes false and the model gets unstable. Therefore, it is necessary to find a value of a leading, for a given temperature, to phase segregation, but small enough to allow the growth of a Rayleigh–Taylor instability. This requirement restricts the ideal range of parameter a to 6.93–7.2, where appreciable changes in the behaviour of the instability can be observed when a is changed by some hundredths, as shown in Fig. 4, exemplifying the requirement of an exhaustive parameter search and fine fitting.

Next, we were interested in the effect of the Atwood number on the evolution rate of the instability. For this purpose, we consider the approach made by Drazin [14], assuming the temporal evolution of the RTI amplitude as $h(t) = h_0 \exp \gamma t$, where $h(t)$ is the time-dependent amplitude of the instability, h_0 is the initial amplitude and

$$\gamma = \sqrt{Agk} \tag{30}$$

is the growing rate, which is a function of the Atwood number, the gravity g, and the wavelength of the perturbation. The growing rate can be estimated by counting the time t needed by the instability to reach certain fixed amplitude as $\gamma \propto 1/t$. Thus, we expect a linear relation between the quantities in the graph (t^2 vs. A^{-1}). As Fig. 4 shows, the linear relation follows for high Atwood numbers, but not for the lowest ones. A possible explanation could be that, at low Atwood numbers, the effect of shear velocities and secondary instabilities is more representative and could change the rate of evolution of the Rayleigh–Taylor instability. Actually, this has been experimentally studied only in 2013 by Akula, Andrews and Ranjan [15], who found that shear effects in Rayleigh–Taylor instability increase the evolution rate for low Atwood Numbers, in agreement with Fig. 5. This is a current field of experimental research and demands a thorough study. The pertinent modification of Eq. (30) is still unknown.

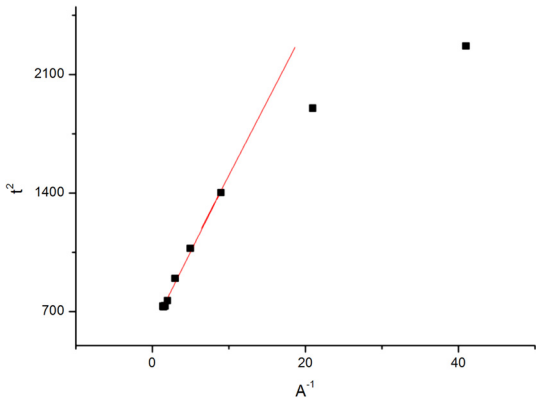

Fig. 5. (Colour online.) Effect of the Atwood number on the evolution rate of the Rayleigh–Taylor instability.

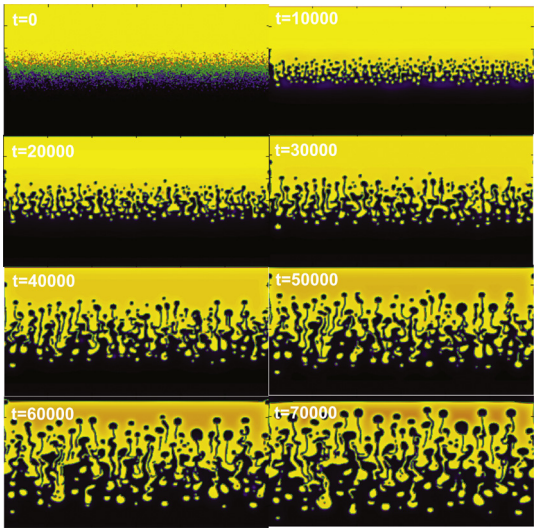

Fig. 6. (Colour online.) Evolution of the multi-mode Rayleigh–Taylor instability.

Simulations of the Rayleigh–Taylor instability with multi-mode initial perturbation were also performed, as shown in Fig. 6. Note that the initial perturbations with larger amplitudes evolve faster than others, as in realistic fluids.

To study the Kelvin–Helmholtz instability, we generated shear velocities between two fluids by defining the following initial conditions for velocity and density, respectively:

$$\boldsymbol{U}(x) = \begin{cases} 0.01\hat{j} & \text{for } x > L_x/2 \\ -0,01\hat{j} & \text{for } x < L_x/2 \end{cases} \tag{31}$$

and

$$\rho(x) = \begin{cases} 1.02 & \text{for } x > L_x/2 \\ 1.0 & \text{for } x < L_x/2 \end{cases} \tag{32}$$

Motivated by the results obtained for the Rayleigh–Taylor instability, we study the effect of the Atwood number on the Kelvin–Helmholtz instability. The comparisons for four different Atwood numbers is shown in Fig. 7. As expected, lower Atwood numbers lead to more symmetrical Kelvin–Helmholtz instabilities and to a better interpenetration between fluids, strengthening our hypothesis about the deviation of the theoretical values in Fig. 5.

4. Conclusions

This work implements a forced multiphase lattice-Boltzmann model for simulating both the Rayleigh–Taylor and Kelvin–Helmholtz instabilities. The model is the one proposed by He, Chen and Zhang [1], which uses an index function to keep a sharp interface between phases, but following the hybrid scheme proposed by McCracken and Abraham [2] to compute the excess pressure gradient, in order to increase accuracy and stability. The model reproduces both instabilities with the

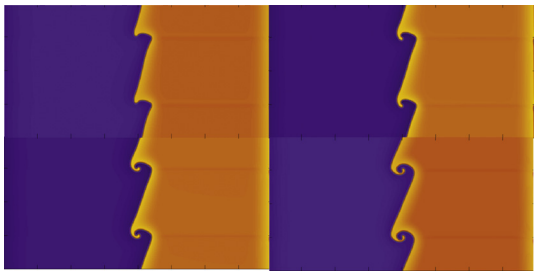

Fig. 7. (Colour online.) Densities from the Kelvin–Helmholtz instability after 3000 time steps for Atwood numbers: 0.5, 0.3, 0.2 and 0.01 (left to right and up to down).

same parameters, which, therefore, can be considered part of the fluid description only. It also fulfils Maxwell's equal-area rule and (without capillarity) shows constant pressure at both sides of the interface, a condition that is maintained over the whole simulation run.

Rayleigh–Taylor instability was simulated by imposing a sinusoidal initial condition. The relation between the wavenumber and the growing rate of the instability shows a similar shape compared with theoretical results, but with a shift of the maximum even when the mesh size is greater. This shift may be due to the order of approximation of the velocity scheme. Whether the problem were to be solved or not by including third-order terms is left for future works. Moreover, the convergence of the numerical scheme requires a thorough analysis.

A strong dependence of the evolution of the RTI with the attractive force parameter of the equation of state was also found; in fact, attractive parameters below 6.93 lead to unstable simulations, because the low-velocity assumption is violated by the rapid increasing of the bubble. By contrast, very high attractive parameters avoid the mixture of the fluids, and then, instability cannot be observed.

The effect of the Atwood number on the rate of evolution of the instability follows the theoretical expression only for high Atwood numbers; deviations at low numbers have been recently found by experimentalists [15]. One possible explanation is the onset of secondary Kelvin–Helmoltz instabilities, which are more representative at low Atwood numbers and could increase the rate of evolution of the Rayleigh–Taylor instability. Our studies on the Kelvin–Helmholtz instability show, indeed, that low Atwood numbers enhance instability, which strengthen the hypothesis that Kelvin–Helmholtz instabilities are the cause of the increased evolution rate of the Rayleigh–Taylor one.

Our results give a fixed set of parameters that can be used as a starting point to simulate other instabilities in more complex geometries, like the radial Rayleigh–Taylor instability or the Rayleigh–Plateau one (as far as surface tension is added to the model by setting $\kappa \neq 0$). But also, it would be of interest to extend this method to larger Reynolds numbers, either by using Multiple Relaxation Times [2] or entropic [10] approaches, in order to simulate, for example, the Richtmyer–Meshkov instability. These interesting topics are left for future research.

Finally, this work illustrates the potentiality of lattice-Boltzmann models to simulate hydrodynamic instabilities, and encourages its use for future applications on these and other non-linear systems.

References

[1] X. He, S. Chen, R. Zhang, A lattice Boltzmann scheme for incompressible multiphase flow and its application in simulation of Rayleigh–Taylor instability, J. Comput. Phys. 152 (1999) 642.
[2] M. McCracken, J. Abraham, Multiple-relaxation-time lattice-Boltzmann model for multiphase flow, Phys. Rev. E 71 (2005) 036701.
[3] X. Shan, H. Chen, Lattice Boltzmann model for simulating flows with multiple phases and components, Phys. Rev. E 47 (1993) 1815.
[4] X. He, X. Shan, G. Doolen, Discrete Boltzmann equation model for nonideal gases, Phys. Rev. E 57 (1998) R13.
[5] X. He, G. Doolen, Thermodynamic foundations of kinetic theory and lattice Boltzmann models for multiphase flows, J. Stat. Phys. 107 (2002) 309.
[6] A. Xu, G. Zhang, Y. Gan, F. Chen, X. Yu, Lattice Boltzmann modeling and simulation of compressible flows, Front. Phys. 7 (5) (2012) 582.
[7] P. Bhatnagar, E. Gross, M. Krook, A model for collision process in gases. I. Small amplitude processes in charged an neutral one component system, Phys. Rev. 94 (1954) 511.
[8] Paulo C. Philippi, Luiz A. Hegele, Luís O.E. dos Santos, Rodrigo Surmas, From the continuous to the lattice Boltzmann equation: the discretization problem and thermal models, Phys. Rev. E 73 (2006) 056702.
[9] N. Martys, A BBGKY-based density gradient approximation of interparticle forces: application for discrete Boltzmann methods, Physica A 362 (2006) 57.
[10] B. Boghosian, J. Yepez, P. Coveney, A. Wager, Entropic lattice Boltzmann methods, Proc. R. Soc. Lond. A 457 (2001) 717.
[11] A. Wagner, Thermodynamic consistency of liquid-gas lattice Boltzmann simulations, Phys. Rev. E 74 (2006) 056703.
[12] D.N. Siebert, P.C. Philippi, K.K. Mattila, Consistent lattice Boltzmann equations for phase transitions, Phys. Rev. E 90 (2014) 053310.
[13] S. Chandrasekhar, Hydrodynamic and Hydromagnetic Stability, Oxford University Press, Oxford, UK, 1961, p. 445.
[14] P. Drazin, Introduction to Hydrodynamic Stability, Cambridge Text in Applied Mathematics, 2002, p. 51.
[15] B. Akula, M. Andrews, D. Ranjan, Effect of shear on Rayleigh–Taylor mixing at small Atwood number, Phys. Rev. E 87 (2013) 033013.